J Mater Sci: Mater Electron (2016) 27:7425–7432
DOI 10.1007/s10854-016-4718-8

Enhanced formaldehyde gas sensing properties of La-doped SnO_2 nanoparticles prepared by ball-milling solid chemical reaction method

Xu xiang[1] · Dachuan zhu[1] · Daji wang[1]

Received: 15 January 2016 / Accepted: 21 March 2016 / Published online: 24 March 2016

Abstract Pure and La-doped SnO_2 nanoparticles were synthesized by ball-milling solid chemical reaction method. The microstructure, morphologies and gas sensing properties of as-synthesized nanoparticles were characterized by X-ray diffraction, scanning electron microscopy, energy dispersive X-ray, transmission electron microscope and gas-sensing measurement device. Compared with pure SnO_2 sensor, La-doped SnO_2 sensor exhibited excellent formaldehyde sensing properties at the optimum temperature of 240 °C. Among them, 3 at% La-doped SnO_2 sensor showed the highest response of 31.5–50 ppm formaldehyde vapor, the response and recovery time were 5 and 26 s, respectively. Moreover, the relationships between response value and HCHO concentration, and the selectivity of pure and 3 at% La-doped SnO_2 sensor were investigated. The result indicated that the 3 at% La-doped SnO_2 sensor had high response, short response-recovery time and good selectivity to formaldehyde. Finally, the gas-sensing mechanism of SnO_2 sensor were discussed.

1 Introduction

Formaldehyde is considered as one of the most common toxic volatile organic compounds (VOC) in homes, offices and urban environment [1]. In recent years, the formaldehyde is widely applied in the field of architecture and decoration, which can lead to the slow release of formaldehyde vapor into the environment [2]. Previous study showed that long-term exposure to the air containing toxic VOC such as formaldehyde, benzene, even led to malignant diseases such as cancer, leukemia, etc. [3]. Hence it is necessary to carry out effective ways to monitor formaldehyde gas in the environment.

Metal oxides semiconductor (MOS), such as SnO_2, ZnO, TiO_2, WO_3, In_2O_3, and so on, is believed to be an ideal material to detect the toxic and flammable gases, and has been developed rapidly because of its low cost, reliability, accuracy and real time gas analyzing [4–8]. Among them, SnO_2, an important n-type semiconductor with a wide band gap energy of 3.6 eV [9], has been proven to be a kind of excellent gas-sensing material with high response to ppm (part per million) level and employed for detection of numerous gases [10]. However, there are some disadvantages in the pristine SnO_2 gas sensor, such as poor selectivity, long response-time and high working temperature, these defects restrict the further application of SnO_2. In order to improve the properties of SnO_2 sensor material, introduction of dopants in the host material is commonly adopted. Many studies have reported the effect of doping of different element (Au [11], Cu [12], Cd [13], Yb [14], Pr [15], Pd [16], Ce [17]) on the structure, morphology and gas sensing properties of SnO_2. Among them, the rare earth doped tin oxide exhibited excellent gas sensing properties due to the unique catalytic and sensitive. Wu et al. [18] have reported that the sensitivity of single crystal SnO_2 nanobelts to ethanediol, ethanol and acetone was enhanced by lanthanum doping. Jinkawa et al. [19] reported the gas-sensing properties of SnO_2 were dramatically enhanced after impregnation of La_2O_3. In general, the doped La_2O_3 has been shown to effectively promote performance of SnO_2 based gas sensors. However, the effects of La-doped SnO_2 on the formaldehyde gas sensing properties is less reported.

✉ Dachuan zhu
zhudachuan@scu.edu.cn

[1] College of Material Science and Engineering, Sichuan University, Chengdu 610065, Sichuan, People's Republic of China

In this paper, we present a simple ball-milling solid chemical reaction approach to synthesize pure and La-doped SnO_2 gas sensor, expecting to enhance the formaldehyde gas sensing properties. The microstructure, morphologies and gas sensing properties of pure and La-doped SnO_2 nanoparticles were studied.

2 Experimental

2.1 Materials

All the chemicals were purchased from Kelong Co, Chengdu, China and used without further processing or purification: chloride dihydrate ($SnCl_2{\cdot}2H_2O$, ≥99 %, AR), oxalic acid dihydrate ($C_2H_2O_4{\cdot}2H_2O$, ≥99 %, AR), Lanthanum nitrate hexahydrate [$La(NO_3)_3{\cdot}6H_2O$, ≥99 %, AR], anhydrous ethanol (≥99 %, AR), Ammonia solution (AR).

2.2 Preparation of pure SnO_2 and La-doped SnO_2 nanoparticles

Pure and La doped SnO_2 were obtained by the ball-milling solid chemical reaction method at room temperature. The mechanochemical reaction was done in a 250 cm^3 agate ball milling jar containing agate ball (ball-to-reagent mass ratio of 10:1). Specimens in this experiment were synthesized as follows: $SnCl_2{\cdot}2H_2O$, certain amount of $La(NO_3)_3{\cdot}6H_2O$ (0, 1, 2, 3, 4 at%) and $C_2H_2O_4{\cdot}2H_2O$ were put into an agate ball milling jar. In addition, the anhydrous ethanol was added to the above system as grinding aid. Subsequently, the milling jar was rotated at 400 rpm in a QM-3SP2 planetary ball mill for 4 h. Meanwhile, ammonia solution was used to adjust the pH of the system per half an hours until pH ≥ 6.5. The product of the mechanochemical reaction (precursor) was ultrasonic washed with distilled water and then ethanol. After washed, the precursor was dried at 70 °C for 12 h. Then, the dry precursor was ground into powder and thermal decomposed at 600 °C for 2 h in muffle furnace to form SnO_2. The possible formation process of SnO_2 samples can be expressed as following chemical equations:

$$SnCl_2 + H_2C_2O_4 \rightarrow SnC_2O_4 + 2HCl \quad (1)$$

$$SnC_2O_4 + O_2 \rightarrow SnO_2 + 2CO_2 \uparrow \quad (2)$$

2.3 Characterization

The X-ray diffraction (XRD) patterns of pure and La-doped SnO_2 were obtained by X-ray diffractometer (XRD-6000, SHIMADZU) using Cu-Kα radiation (λ = 1.5418 Å). A continuous scan mode was used to collect 2θ data from 20° to 80°. Scanning electron microscope (SEM: JEOL JSM-5900LV, Japan) was used to observe the morphology of calcined samples and the energy dispersive X-ray (EDX) technique was used to determine their elemental compositions. Transmission electron microscope (TEM) images were taken by using JEOL JEM-100CX (Japan).

2.4 Fabrication and measurement of gas sensor

The basic fabricated process of gas sensor is as follows: The as-prepared SnO_2 powders and a suitable amount of anhydrous ethanol were mixed and then ultrasonic dispersed to form a paste. Then the paste was coated on ceramic tubes, on which a pair of Au electrodes and four Pt wires were previously installed at each end. The coated ceramic tubes were calcined at 300 °C for 2 h. Subsequently, a heater of Ni–Cr wire was inserted into the ceramic tube to regulate the working temperature (Fig. 1a). The sensor devices were aged for 5 days in air in order to improve the long-term stability.

The gas-sensing properties were measured by a WS-30A gas sensitivity instrument (Weisheng Electronics Co., Ltd China). Figure 1b displayed the basic measuring electric circuit of gas sensing characteristics. The sensor response was defined as $S = R_a/R_g$, where R_a and R_g are separately the electrical resistance of the sensor in air and test gas. The response time was defined as time reaching the 90 % steady response value and the recovery time was defined as time attaining within 10 % of the initial response value [15].

3 Results and discussion

3.1 Structural and morphological characteristics

Figure 2a shows the typical XRD patterns of pure and La-doped SnO_2 sample, all diffraction peaks can be indexed to tetragonal rutile SnO_2 phase (JCPDS NO. 41-1445,

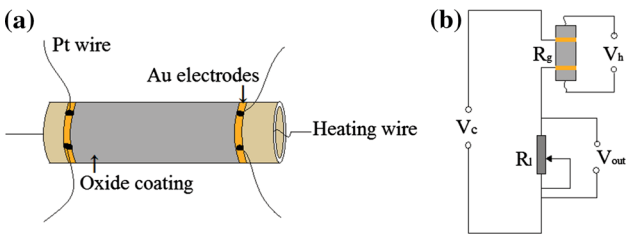

Fig. 1 Schematic illustration of **a** the gas sensor and **b** the electrical circuit for the gas sensing test (V_h heating voltage, V_c circuit voltage, V_{out} signal voltage, R_l load resistor)

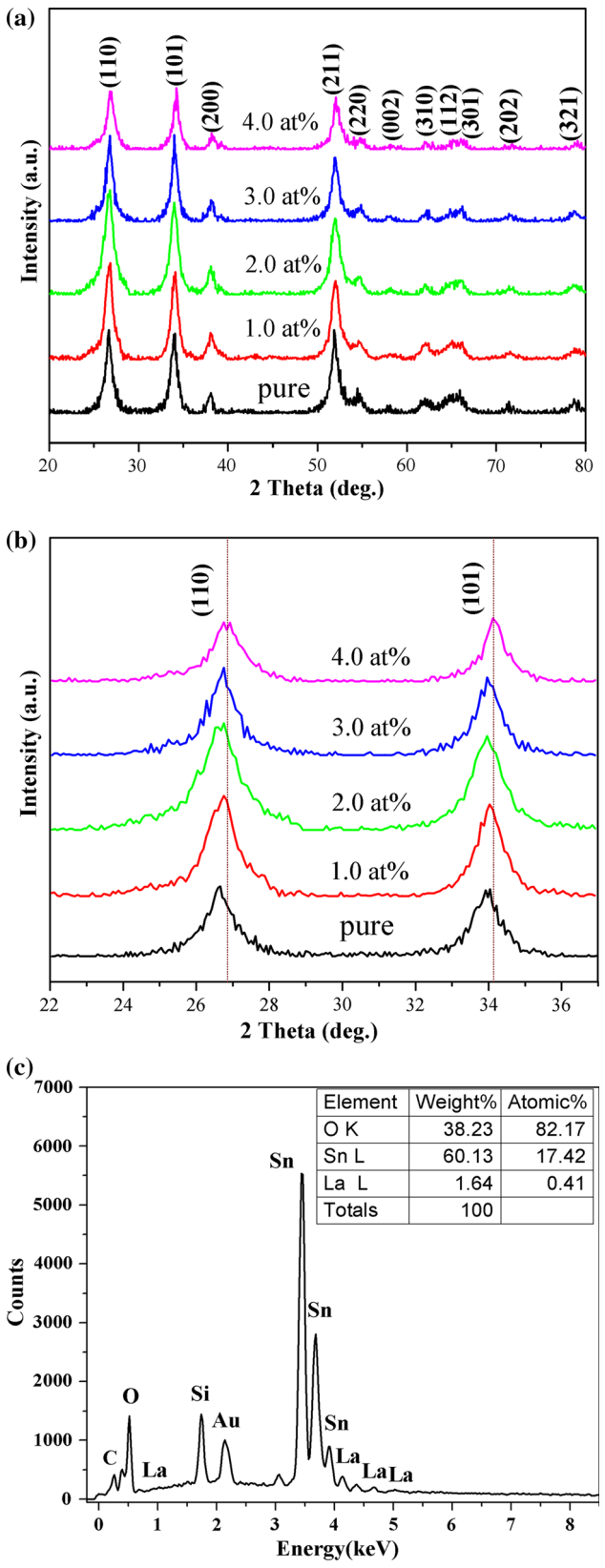

Fig. 2 **a** XRD pattern of SnO_2 with different doping amount of La. **b** Comparison the shift of (110) and (101) peaks. **c** The EDX pattern of 3.0 at% La-doped SnO_2

a = b = 4.7382 Å, c = 3.1871 Å) [20, 21]. However, no diffraction peaks of La can be obviously observed, which is probably because addition of La is low so as to dissolve in SnO_2 lattice [14]. The average size estimated by full width at half maximum (FWHM) of (110) using Scherrer's formula is 9.1, 8.3, 7.9, 8.7, 10.7 nm, corresponding to the La-doped content of 0, 1, 2, 3 and 4 %. To further discuss the effect of La doping on structure characteristics of SnO_2, the (110) and (101) diffraction peaks of sample are magnified in Fig. 2b. For all the La-doped sample, it can be seen that the 2θ diffraction peaks shift to the bigger angle side compared to the pure SnO_2. According to the Bragg's law and the tetragonal rutile structure of SnO_2 system, the lattice constant a of samples can be calculated and simplified as the following formula [22]:

$$a = \frac{\lambda}{\sqrt{2}sin\ \theta} \tag{3}$$

where λ and θ are separately the X-ray wavelength (0.15418 nm) and diffraction angle of (110) crystal lattice plane. Table 1 shows the 2θ position of prominent diffraction peaks and lattice parameter calculated from Eq. (3). It is observed that diffraction angles of the (110), (101) and (211) peaks increase and the lattice constant a gradually decreases with the increase of La doping. Both the shift of diffraction peaks and decrease of lattice constant a probably prove that La doping can cause lattice mismatch of SnO_2. Figure 2c shows the corresponding EDX pattern of 3.0 at% La-doped SnO_2 powder. As can be seen, the as-synthesized product is consisted of O, Sn and La elements. The additional peaks of C, Si and Au are caused in the detection process. All of these suggest that the lanthanum ions have been doped into SnO_2 lattice.

Figure 3a–e displays the SEM images of SnO_2 powder doped with different amount of La. It can be seen that the La doping has little impact on morphology of SnO_2. This is possibly because in the ball-milling solid chemical reaction, mechanical force makes the refinement degree of precursor particles tend to be consistent. Both the pure and La-doped SnO_2 powders consist of aggregation of spherical shaped particles and the size of aggregations is in range of 50–500 nm.

Figure 4 gives the TEM image of 3 at% La-doped SnO_2 powder. We can see that the aggregations mentioned above are gathered from the nanoparticles with a size of about 14 nm. The crystallite size from TEM is in good with the XRD results.

3.2 Gas sensing properties

Many studies have proven that the gas sensitivity is greatly influenced by the operating temperature [23–26]. In order to determine the optimum operating temperature for

formaldehyde detection, the responses of pure and La-doped SnO_2 sensors to 100 ppm HCHO at different operating temperature are tested as shown in Fig. 5. As the operating temperature rises, the response performances of

Table 1 A list of 2θ position and lattice constant a of pure and La-doped SnO_2

	0 at%	1 at%	2 at%	3 at%	4 at%
110	26.658	26.750	26.751	26.757	26.769
101	33.927	34.04	33.959	33.970	34.273
211	51.896	51.949	51.957	52.034	52.043
a (Å)	4.7289	4.7129	4.7128	4.7117	4.7097

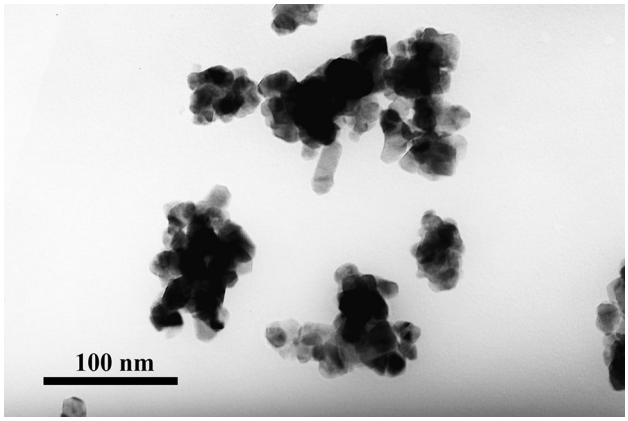

Fig. 4 TEM images of 3 at% La-doped SnO_2 nanoparticles

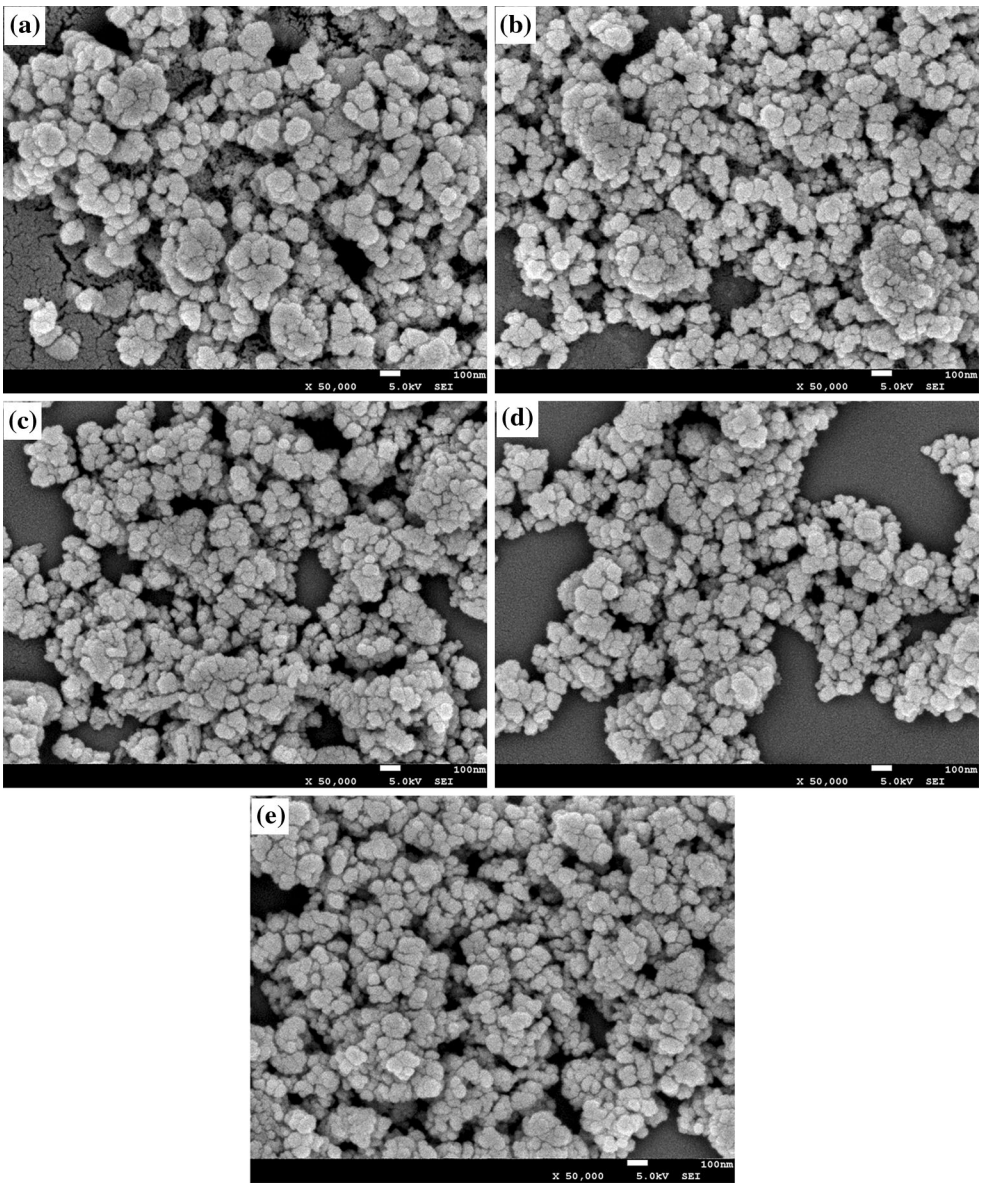

Fig. 3 SEM images of **a** pure and **b** 1 at%, **c** 2 at%, **d** 3 at%, and **e** 4 at% La-doped SnO_2 nanoparticles

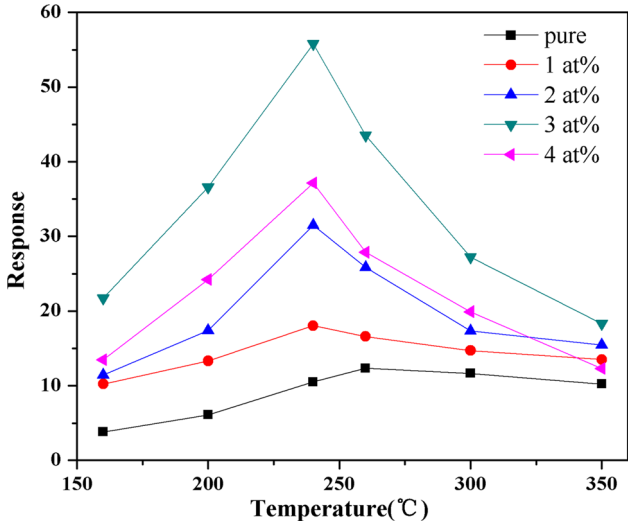

Fig. 5 Response of pure and La-doped SnO_2 sensors to 100 ppm HCHO at different operating temperature

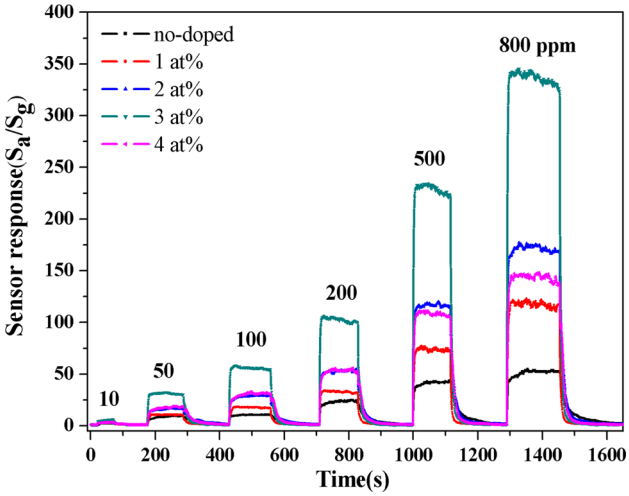

Fig. 6 The response and recovery characteristic curves of pure and La-doped SnO_2 sensors to formaldehyde vapor at 240 °C

all sensors are enhanced at first and reach the maximum value at 240 °C, then decrease gradually with a further rising of temperature. Therefore, the optimum working temperature of La-doped SnO_2 sensors towards formaldehyde is 240 °C.

Figure 6 shows the response and recovery characteristic curves of pure and La-doped SnO_2 sensors to formaldehyde vapor at 240 °C. The concentration range of formaldehyde vapor is 10–800 ppm, and the relative humidity is 55 % RH. It can be seen from the figure that the response cycles corresponding to the 10, 50, 100, 200, 500 and 800 ppm, are recorded successively. The continuity of response and recovery characteristic curve is good, demonstrating the sensors have good repeatability and stability [12]. In addition, the response value of undoped SnO_2 sensor is obviously lower than that of those sensors with different amount of La-doping. It shows that La doping can effectively improve the HCHO gas sensing properties of SnO_2 sensor. Among all these La-doped SnO_2 sensors, the one with 3 at% La-doped shows the highest response value to different concentrations of formaldehyde gas. Therefore, the optimum amount of La-doping to HCHO gas-sensing for this work is 3.0 at%. Moreover, the response value and response-recovery time (Tres/Trec) of (0, 3 at%) La-doped SnO_2 sensors to 50, 100, 200, and 500 ppm formaldehyde vapor are listed in Table 2. The average response and recovery time of (0, 3 at%) La-doped SnO_2 sensors is about 25, 5 and 100, 26 s, respectively, which indicates that the doping of La can significantly shorten the response and recovery time.

Figure 7 shows the response of 3 at% La-doped SnO_2 sensor versus formaldehyde concentration from 5 to 6000 ppm at 240 °C. When exposed to 5 ppm HCHO, the response value of 3 at% La-doped SnO_2 sensor is 4.2, suggesting it has good gas sensing properties in the lower formaldehyde concentration and the detectable minimum limit is about 5 ppm. On the other hand, the response rises up rapidly with increasing formaldehyde concentration, especially in the range of 0–200 ppm, the relationship between the sensor response and HCHO concentration is linear ranging (as shown in the inset of Fig. 7). But the rising rate is reduced when the concentration of formaldehyde vapor exceeds 800 ppm, which illustrates that the sensor tends to saturation gradually [21]. Furthermore, Fig. 8 exhibits the corresponding dynamic resistances change of pure and 3 at% La-doped SnO_2 sensor at 240 °C in the logarithmic coordinates. The resistance of pure and 3 at% La-doped SnO_2 sensor is about 481 and 9625 kΩ in air. When the formaldehyde is introduced, the resistance drops sharply.

Besides, the selectivity is one of the key parameters for appraising the properties of gas sensors [27–29]. In order to clarify the selectivity of our sample, the pure and 3 at% La-doped SnO_2 sensors are tested in various gases, such as ethanol (EtOH), acetone (CH_3COCH_3), ammonia (NH_3) and formaldehyde (HCHO) of 500 ppm at 240 °C. As shown in Fig. 9. It can be observed clearly that the 3 at% La-doped SnO_2 sensor shows a higher response to all the tested gas than pure SnO_2. Moreover, the response of 3 at% La-doped SnO_2 sensor to HCHO is about 233, which is much higher than that to other test gases. The result demonstrates the 3 at% La-doped SnO_2 sensor has a good selectivity to formaldehyde.

To sum up, 3 at% La-doped SnO_2 sensor has high response, short response-recovery time and good selectivity to formaldehyde. A comparison of this work with other

Table 2 The performance of SnO_2 sensors towards different concentrations of HCHO gases

	50 ppm		100 ppm		200 ppm		500 ppm		Average T_{res}/T_{rec}
	Response	T_{res}/T_{rec}	Response	T_{res}/T_{rec}	Response	T_{res}/T_{rec}	Response	T_{res}/T_{rec}	
0 at%	9.3	32/106	10.1	14/92	10.1	27/113	43	23/86	25/100
3 at%	31.5	5/23	58.2	4/24	104	4/28	233	4/31	5/26

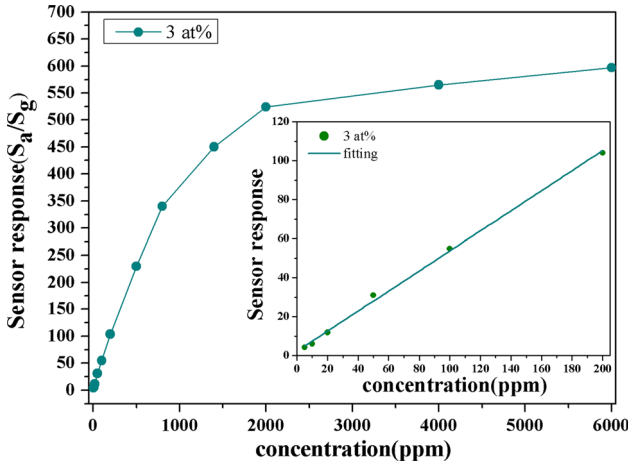

Fig. 7 3 at% La-doped SnO_2 sensor versus formaldehyde concentration from 5 to 6000 ppm at 240 °C

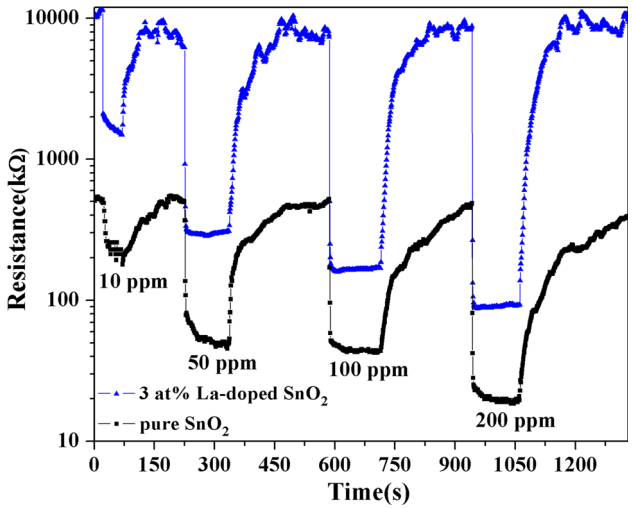

Fig. 8 The dynamic resistance change of pure and 3 at% La-doped SnO_2 sensor toward to 10, 50, 100 and 200 ppm formaldehyde at 240 °C

formaldehyde sensors based on SnO_2 material using various methods is presented in Table 3. The result shows that the 3 at% La-doped SnO_2 is a promising candidate for formaldehyde sensor related applications.

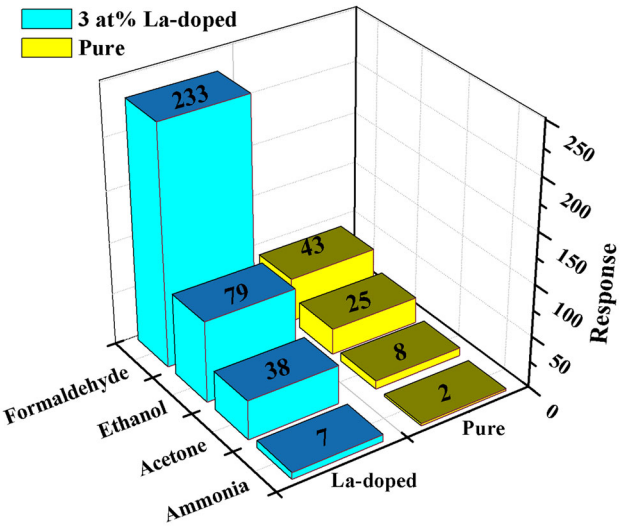

Fig. 9 Response of pure and 3 at% La-doped SnO_2 sensor to 500 ppm different gases at 240 °C

3.3 Gas sensing mechanism

As a kind of surface-control type sensing material, gas sensing performance of SnO_2 is mainly influenced by its surface characteristics. Monitoring of the target gas concentration by SnO_2 gas sensor is dependent on the change of surface resistance. When pure SnO_2 is exposed to air, oxygen molecules tend to be adsorbed on the surface, and then the partially adsorbed oxygen will capture electrons from the surface to generate ions in the form of $O^-_{2(ads)}$, $O^-_{(ads)}$ and $O^{2-}_{(ads)}$. The process is as follows [10, 18, 28]:

$$O_{2(gas)} \rightarrow O_{2(ads)} \quad (4)$$

$$O_{2(ads)} + e^- \rightarrow O^-_{2(ads)} \quad (5)$$

$$O^-_{2(ads)} + e^- \rightarrow 2O^-_{(ads)} \quad (6)$$

$$O^-_{(ads)} + e^- \rightarrow O^{2-}_{(ads)} \quad (7)$$

These adsorbed oxygen ions can cause a reduction of electron concentration in the conduction band, resulting in the formation of potential barrier [2]. Thus, the resistivity of SnO_2 in air is higher than the intrinsic resistivity.

Table 3 Various metal oxide semiconductor gas sensors to HCHO surveyed in literatures

Material	Method	T^{a}_{opt} (°C)	Sensor response	T_{res}/T_{rec} (s)	References
Au@SnO_2 core–shell	sol–gel	RT	2.9 (50 ppm)	80/62 (50 ppm)	[11]
Cu-doped SnO_2 nanoparticles	Co-precipitation	200	5.1 (50 ppm)	–/–[b]	[30]
SnO_2–graphene nanocomposite	In situ solid-state chemical reaction	260	35 (100 ppm)	–/–	[31]
Sn–ZnO thin film	Spray pyrolysis	300	18.2 (100 ppm)	180/170 (100 ppm)	[24]
Electrospun NiO–SnO_2 nanofibers	Electrospinning	200	14 (50 ppm)	50/80 (10 ppm)	[32]
Pd–SnO_2 thin films	Sol–gel	250	1.5 (10 ppm)	50/– (10 ppm)	[33]
SnO_2/In_2O_3 hetero-nanofibers	Electrospinning	375	18.9 (50 ppm)	30/– (10 ppm)	[34]
La-SnO_2 nanoparticles	Ball-milling solid chemical reaction	240	31.5 (50 ppm)	5/23 (50 ppm)	This work

[a] T_{opt} means optimum operating temperature

[b] Means the corresponding information is not mentioned in the original

However, when SnO_2 is exposed to a reducing gas such as HCHO, the reducing gas molecules will react with adsorbed oxygen ions and release the trapped electrons to conduction band [14]. As a result, the conductivity increases and potential barrier height reduction. The process may be carried out by Eq. (8) [2, 16, 24].

$$\mathrm{HCHO} + 2O^{-}_{(ads)} \rightarrow CO_2 + H_2O + 2e^{-} \quad (8)$$

As the working temperature rises, the carrier concentration in the conduction band of SnO_2 and the chemical activation increase lead to an improvement of response value. But when the temperature is too high, the adsorbed reducing gas molecules may escape from the surface of the sensor [15], resulting in a poor response. Therefore, the gas sensors exhibited the highest response at 240 °C,

According to the XRD analysis mentioned above, as well as the ionic radii of La^{3+} (0.103 nm) is larger than that of Sn^{4+} (0.071 nm), it is reasonable to consider that the lanthanum ions doped into the SnO_2 lattice induced lattice mismatch. This could provide more active sites on the surface of SnO_2 to adsorb more oxygen, which greatly raises the resistivity of SnO_2 in air, this result can be demonstrated from Fig. 8. On the other hand, the increase of active sites is beneficial to the decomposition of HCHO, which makes more trapped electrons released, resulting in the decrease of resistivity in reducing gas. Ultimately, the response of SnO_2 sensors is enhanced. In addition, La_2O_3, as the ultimate doping production, is favorable to produce O_2^{2-} on its surface. The O_2^{2-} could trigger an H-abstraction chemical reaction with hydrocarbon compound [35]. Therefore, when formaldehyde gas is introduced, the reaction energy of oxidation of carbon-hydrated is reduced and the response of La-doped SnO_2 sensor is enhanced. Finally, with the concentration of formaldehyde gas increasing, more electrons are released, and the response value rises continuously. Until adsorbed oxygen ions are depleted, the sensors become saturation, as shown in the Fig. 7.

When the lanthanum doping concentration exceeds 3 at%, the response value decreases, this may be because the redundant doping will lead to the formation of many clusters such as La–La or La–O, reducing the electric transduction of SnO_2 nanoparticles [14]. In addition, an excess of lanthanum doping may cause the abnormal growth of SnO_2 crystallite and the decrease of specific surface area, it can be seen in the results of XRD. This may be another reason why the response value decreases in the 4 at% La-doped SnO_2 sensor.

4 Conclusions

In conclusion, pure and La-doped SnO_2 nanoparticles are successfully synthesized by ball-milling solid chemical reaction method and studied for the detection of formaldehyde vapor. We find that at the optimum operating temperature of 240 °C, the La-doped SnO_2 sensors exhibit the enhanced HCHO sensing properties comparing with the pure SnO_2 sensor. Especially, 3 at% La-doped SnO_2 sensor shows the highest response to formaldehyde gas. The improvement of gas-sensing properties of SnO_2 sensor is attributed to the increase of active sites and the production of O_2^{2-} ion. Furthermore, compared with previous studies, the 3 at% La-doped SnO_2 sensor shows high response, short response-recovery time and good selectivity to formaldehyde, indicating that 3 at% La-doped SnO_2 can be a promising candidate for formaldehyde sensor.

Acknowledgments The authors are grateful for the Project 2014GZ0090 supported by the Science and Technology Support Program in Sichuan.

References

1. C.J. Weschler, Atmos. Environ. **43**, 153 (2009)
2. Y. Lin, Y. Wang, W. Wei, L.H. Zhu, S.P. Wen, S.P. Ruan, Ceram. Int. **41**, 7329 (2015)
3. J.Y. Chen, Y. Huang, G.Y. Li, T.C. An, Y.K. Hu, Y.L. Li, J. Hazard. Mater. **302**, 395 (2016)
4. D.Z. Zhang, J.J. Liu, H.Y. Chang, A.M. Liu, B.K. Xia, RSC Adv. **5**, 18666 (2015)
5. S. Sarkar, D. Basak, Sens. Actuators B Chem. **176**, 374 (2013)
6. N. Kılınç, E. Şennik, Z.Z. Öztürk, Thin Solid Films **520**, 953 (2011)
7. X.H. Ding, D.W. Zeng, S.P. Zhang, C.S. Xie, Sens. Actuators B Chem. **155**, 86 (2011)
8. S. Yi, S.Q. Tian, D.W. Zeng, K. Xu, S.P. Zhang, C.S. Xie, Sens. Actuators B Chem. **185**, 345 (2013)
9. S.C. Yeow, W.L. Ong, A.S.W. Wong, G.W. Ho, Sens. Actuators B Chem. **143**, 295 (2009)
10. L.P. Chikhale, J.Y. Patil, A.V. Rajgure, F.I. Shaikh, I.S. Mulla, S.S. Suryavanshi, Ceram. Int. **40**, 2179 (2014)
11. F.C. Chung, R.J. Wu, F.C. Cheng, Sens. Actuators B Chem. **190**, 1 (2014)
12. W.X. Jin, S.Y. Ma, Z.Z. Tie, J.J. Wei, J. Luo, X.H. Jiang et al., Sens. Actuators B Chem. **213**, 171 (2015)
13. Z. Tianshu, P. Hing, Y. Li, Z. Jiancheng, Sens. Actuat B Chem. **60**, 208 (1999)
14. T.T. Wang, S.Y. Ma, L. Cheng, J. Luo, X.H. Jiang, W.X. Jin, Sens. Actuators B Chem. **216**, 212 (2015)
15. W.Q. Li, S.Y. Ma, Y.F. Li, X.B. Li, C.Y. Wang, X.H. Yang et al., J. Alloys Compd. **605**, 80 (2014)
16. N. Ma, K. Suematsu, M. Yuasa, K. Shimanoe, ACS Appl. Mater. Interfaces **7**, 15618 (2015)
17. W.F. Qin, L. Xu, J. Song, R.Q. Xing, H.W. Song, Sens. Actuators B Chem. **185**, 231 (2013)
18. Y.M. Wu, H. Zhang, Y.K. Liu, W.W. Chen, J. Ma, S.H. Li et al., Sensors **15**, 14230 (2015)
19. T. Jinkawa, G. Sakai, J. Tamaki, N. Miura, N. Yamazoe, J. Mol. Catal. A: Chem. **155**, 193 (2000)
20. W. Zeng, H. Zhang, Y.P. Li, W.G. Chen, Z.C. Wang, Mater. Res. Bull. **57**, 91 (2014)
21. W.X. Jin, S.Y. Ma, Z.Z. Tie, W.Q. Li, J. Luo, L. Cheng, X.L. Xu et al., Appl. Surf. Sci. **353**, 71 (2015)
22. F.C. Yang, Z.G. Guo, J. Colloid Interface Sci. **448**, 265 (2015)
23. H. Yu, S.M. Wang, C.H. Xiao, B.X. Xiao, P. Wang, Z.F. Li et al., CrystEngComm **17**, 4316 (2015)
24. C.S. Prajapati, A. Kushwaha, P.P. Sahay, Appl. Phys. A **113**, 651 (2013)
25. S.Q. Tian, X.H. Ding, D.W. Zeng, S.P. Zhang, C.S. Xie, Sens. Actuators B Chem. **186**, 640 (2013)
26. J.J. Wu, D.W. Zeng, S.Q. Tian, K. Xu, D.G. Li, C.S. Xie, J. Mater. Sci. **50**, 7725 (2015)
27. J.R. Huang, L.Y. Wang, C.P. Gu, Mater. Lett. **136**, 371 (2014)
28. J.P. Du, R.H. Zhao, Y.J. Xie, J.P. Li, Appl. Surf. Sci. **346**, 256 (2015)
29. N. Duc Chinh, N. Van Toan, V. Van Quang, N. Van Duy, N. Duc Hoa, N. Van Hieu, Sens. Actuators B Chem. **201**, 7 (2014)
30. R.K. Mishra, A. Kushwaha, P.P. Sahay, RSC Adv. **4**, 3904 (2014)
31. Y.L. Cao, Y.Z. Li, D.Z. Jia, J. Xie, RSC Adv. **4**, 46179 (2014)
32. Y.G. Zheng, J. Wang, P.J. Yao, Sens. Actuators B Chem. **156**, 723 (2011)
33. J. Wang, P. Zhang, J.Q. Qi, P.J. Yao, Sens. Actuators B Chem. **136**, 399 (2009)
34. H.Y. Du, J. Wang, M.Y. Su, P.J. Yao, Y.G. Zheng, N.S. Yu, Sens. Actuators B Chem. **166–167**, 746 (2012)
35. G.Z. Zhang, S.P. Zhang, L. Yang, Z.J. Zou, D.W. Zeng, C.S. Xie, Sens. Actuators B Chem. **188**, 137 (2013)